REPORT DOCUMENTATION PAGE

Form Approved
OMB No. 0704-0188

PLEASE DO NOT RETURN YOUR FORM TO THE ABOVE ORGANIZATION.

1. REPORT DATE *(DD-MM-YYYY)*	2. REPORT TYPE	3. DATES COVERED *(From - To)*
02 Jun 2008	FINAL REPORT	01 Jun 2005 - 30 Nov 2007

4. TITLE AND SUBTITLE

Image Reconstruction, Wave Front Sensing, and Adaptive Optics in Extreme Atmospheric Seeing Conditions

5a. CONTRACT NUMBER

FA9550-05-1-0404

5b. GRANT NUMBER

5c. PROGRAM ELEMENT NUMBER

6. AUTHOR(S)

Michael C. Roggemann
Timothy J. Schulz

5d. PROJECT NUMBER

5e. TASK NUMBER

5f. WORK UNIT NUMBER

7. PERFORMING ORGANIZATION NAME(S) AND ADDRESS(ES)

Michigan Technological University
1400 Townsend Drive
Houghton, MI 49931

8. PERFORMING ORGANIZATION REPORT NUMBER

9. SPONSORING/MONITORING AGENCY NAME(S) AND ADDRESS(ES)

AF OFFICE OF SCIENTIFIC RESEARCH/NE
875 NORTH RANDOLPH STREET ROOM 3112
ARLINGTON VA 22203

10. SPONSOR/MONITOR'S ACRONYM(S)

11. SPONSOR/MONITOR'S REPORT NUMBER(S)

AFRL-SR-AR-TR-08-0364

12. DISTRIBUTION/AVAILABILITY STATEMENT

DISTRIBUTION STATEMENT A: UNLIMITED

13. SUPPLEMENTARY NOTES

14. ABSTRACT

On June 1, 2005 AFOSR awarded a grant to Michigan Technological University to investigate image reconstruction, wave front sensing, and adaptive optics in extreme imaging conditions. The overall goal is to understand imaging under conditions where seeing is exceedingly poor, such as for space surveillance of objects at very low elevation angles, and during daytime hours. In these situations, scintillation and small isoplanatic angles dominate the image measurement and reconstruction problems We have focused on performing tradeoffs in the adaptive optics control algorithms for imaging under conditions of poor seeing arising from large zenith angles. In particular, we have developed a closed loop simulation of an adaptive optics system which is physically similar to the AEOS system, that uses both the conventional least squares reconstructor, the exponential reconstruction, and the so-called "slope discrepancy" reconstructor.

15. SUBJECT TERMS

16. SECURITY CLASSIFICATION OF:			17. LIMITATION OF ABSTRACT	18. NUMBER OF PAGES	19a. NAME OF RESPONSIBLE PERSON
a. REPORT	b. ABSTRACT	c. THIS PAGE			19b. TELEPHONE NUMBER *(Include area code)*

Reset

Final Report to AFOSR

Image Reconstruction, Wave Front Sensing, and Adaptive Optics in Extreme Atmospheric Seeing Conditions

Grant # FA9550-05-1-0404
Michael C. Roggemann, PI; Timothy J. Schulz, Co-PI
Michigan Technological University
Department of Electrical and Computer Engineering
1400 Townsend Drive
Houghton, MI 49931

Abstract

On June 1, 2005 AFOSR awarded a grant to Michigan Technological University to investigate image reconstruction, wave front sensing, and adaptive optics in extreme imaging conditions. This final report for this program. The overall goal was to understand imaging under conditions where seeing is exceedingly poor, such as for space surveillance of objects at very low elevation angles, and during daytime hours. In these situations, scintillation and small isoplanatic angles dominate the image measurement and reconstruction problems Our work was focused on performing tradeoffs in the adaptive optics control algorithms for imaging under conditions of poor seeing arising from large zenith angles. In particular, we have developed a closed loop simulation of an adaptive optics system which is physically similar to the AEOS system, that uses the conventional least squares reconstructor, the exponential reconstruction, and the so-called "slope discrepancy" reconstructor. We have also examined the use of the stochastic parallel gradient descent (SPGD) algorithm for deformable mirror control in problems dominated by scintillation and anisoplanatism, and conducted a laboratory experiment to demonstrate this idea. In this report we document the results. Our work with maximum likelihood-based image reconstruction algorithms has been applied to the results provided by the adaptive optics simulation, and representative results are included here.

Overview of the Program

The problem we addressed in this program is to develop image measurement and post processing techniques to make useful space surveillance observations in unconventional, and technically demanding conditions. As conventional adaptive optics technology has matured, the space surveillance user community has developed a strong interest in making observations in more challenging imaging conditions, such as during daytime hours, and objects which are at very low elevation angles. Turbulence effects are generally much stronger in these conditions due to, for example, a longer path through the atmosphere for the case of imaging at low elevation angles; and stronger turbulence and high sky background conditions during the daylight hours compared to conventional imaging during terminator conditions. Our approach was based on the following key elements:

1. Theoretical understanding of the problem.
2. High fidelity simulations.

3. Estimation theoretic approach to processing available measurements, reconstructing images.

In the first year we developed a theoretical understanding of the problem, and started extending our simulation capability. In the second year we completed the simulation of wave propagation and imaging through the atmosphere with an adaptive optics telescope similar to AEOS, which we are testing under extreme conditions using, so far, least squares [Roggemann, 1996] and slope discrepancy-based [Tyler, 2000] deformable mirror controllers. In the final year of this project we developed and demonstrated a more efficient implementation of the exponential reconstructor, and completed a detailed comparison of all the reconstructors over a wide range of imaging conditions. We also developed a laboratory experiment in the SPGD area. These results have been documented in a set of conference papers, submitted journal articles, and a dissertation, which are included in this submission. We have also been developing and testing image reconstruction algorithms to work in association with this adaptive optics telescope model.

Among the key findings of this study is that the novel implementation of the exponential reconstructor developed here achieves a performance slightly better than the widely used least squares reconstructor in the lower noise levels simulated. The degree of improvement was also found to increase as the turbulence conditions worsen. This makes the exponential reconstructor a good choice for use in severe turbulence conditions. The slope discrepancy reconstructor was found to perform slightly better than the exponential reconstructor working alone in the lower zenith angles simulated, and this advantage diminishes at the higher zenith angles. This method was implemented taking advantage of the novel implementation of the exponential reconstructor. At the highest noise level simulated, the least squares reconstructor performed better than the exponential reconstructor and the slope discrepancy method by about 1%. This indicates that the exponential reconstructor is more sensitive to noise than the least squares reconstructor.

The SPGD algorithm was successfully demonstrated in both simulation and experiment. It was found through simulation that the algorithm has the potential to perform better than conventional wave front sensing and wave front reconstructors in the most severe conditions tested. If turbulence conditions demand an impractically small wave front sensor subaperture size, the SPGD algorithm may be a good choice. Trials were simulated with the same turbulence profile used for the wave front reconstructors, and at double that turbulence profile. At the standard turbulence profile used for the reconstructors, the performance of SPGD was generally lower than the reconstructors, except at the highest noise level simulated. When the turbulence profile was doubled, SPGD simulations did at least as well as the reconstructors at all noise levels tested. Experimental testing of the SPGD algorithm demonstrated that the algorithm can converge with moving phase screens representing changing turbulence conditions. If the algorithm can be made to run fast enough, the performance approaches the performance achieved with fixed phase screens.

We now present some key results from this work. Also provided as attachments to this report are some publications and a dissertation resulting from this work which provide a more complete coverage of these topics.

The remainder of this report is organized as follows. In the next section we summarize our work in developing and comparing wave front reconstructors which work by

processing wave front sensor measurements. We then present our work with the SPGD algorithm to control the DM in strong turbulence. Finally, we discuss and present some results for using an MFBD approach to image reconstruction based on the expectation maximization (EM) algorithm to reconstruct images output by the adaptive optics system under these conditions.

Wave front reconstructors

As turbulence effects get stronger, the spatial correlation length of the field gets smaller, and amplitude fluctuations referred to as scintillation develop in the field falling on the pupil of the telescope. As a result, the fluctuations of the field are generally undersampled by the wave front sensor, and discontinuities in the surface of constant phase can develop which are referred to as branch cuts. Both of these effects make optimal control of the deformable mirror difficult, and this provides the motivation for this part of our effort.

We implemented three wave front reconstructors in this program: the conventional least squares reconstructor which is most widely used to control adaptive optics systems, a new implementation of the exponential reconstructor which is a more efficient single grid solution than the published two grid technique, and an approach combining the least squares and exponential reconstructor called the slope discrepancy reconstructor. We performed comparative studies of the performance of these reconstructors as a function of zenith angle for the Maui3 turbulence profile and the AEOS telescope and adaptive optics system. Extensive analysis and results are presented in the dissertation by Grant Soehnel, which is attached. The key results are presented in Tables 1, 2, and 3 below.

		Source Visual Magnitude			
		No Noise	2	4	6
Zenith Angle	0	77.19	76.80	72.8	59.77
	30	73.69	73.02	69.12	56.10
	60	54.65	53.96	50.64	38.85
	67	42.62	41.16	35.35	20.03

(a)

		Source Visual Magnitude			
		No Noise	2	4	6
Zenith Angle	0	76.4	75.78	72.51	60.39
	30	72.77	72.17	68.97	56.98
	60	53.17	52.68	50.09	39.85
	67	40.69	39.85	35.68	23.01

(b)

Table 1. Strehl ratios for: (a) Exponential reconstructor; (b) Least squares reconstructor with waffle correction.

		Source Visual Magnitude			
		No Noise	2	4	6
Zenith Angle	0	68.23	67.34	63.43	50.39
	30	64.75	63.92	59.31	46.74
	60	44.97	44.92	41.20	31.32
	67	33.71	33.54	28.75	15.99

(a)

		Source Visual Magnitude			
		No Noise	2	4	6
Zenith Angle	0	77.98	77.10	72.84	59.23
	30	74.91	73.88	69.58	56.22
	60	55.23	54.67	50.61	38.69
	67	42.77	41.55	35.02	20.91

(b)

Table 2. Strehl ratios for: (a) Two grid exponential reconstructor; (b) Slope Discrepancy Method.

		Source Visual Magnitude			
		No Noise	2	4	6
Zenith Angle	0	73.24	72.96	68.58	53.50
	30	68.12	69.20	65.03	50.73
	60	44.53	45.11	42.01	32.05
	67	35.20	34.97	28.97	19.10

Table 3. Strehl ratios for least squares with no wa^2e correction.

Inspection of Tables 1-3 shows that the exponential reconstructor working on the single grid geometry performs better than the least squares method with no noise and with a

magnitude 2 source. This advantage is about a 1-2% higher Strehl ratio. In addition, the slope discrepancy method, which makes use of the single grid implementation of the exponential reconstructor, does produce up to a 1% higher Strehl ratio than the exponential reconstructor working alone. In particular, slope discrepancy produces a 1.58% higher Strehl ratio than least squares with no noise at θ_z = 0, and a 2.08% higher Strehl ratio than least squares with no noise at θ_z = 67. In addition, the 2.08% higher Strehl ratio at values of about 40% is proportionally much larger than the 1.58% higher Strehl ratio at values near 77%. This indicates that the advantage of the exponential reconstructor and slope discrepancy method over least squares grows larger as the zenith angle increases and turbulence conditions worsen. The Strehl ratios achieved with the
least squares reconstructor, the exponential reconstructor, and the slope discrepancy method are all nearly the same with a magnitude 4 source. The least squares reconstructor achieves the highest Strehl ratio with a magnitude 6 source. This indicates that while the exponential reconstructor is able to perform better than the least squares reconstructor in relatively low measurement noise, the exponential reconstructor is more sensitive to noise than the least squares reconstructor. The least squares reconstructor without the waffle correction and the exponential reconstructor working on the two-grid geometry always resulted in lower Strehl ratios than the other three methods. The two grid exponential reconstructor produces more waffle error than least squares, so it generally is the worst method simulated. However, the performance of the two grid exponential
is closer to that of the least squares without the waffle correction at the highest two zenith angles. This is further evidence that the exponential reconstructor performs well in severe turbulence conditions. These results indicate that there are conditions for which the exponential reconstructor is a better choice than the least squares reconstructor. These conditions are when the turbulence distortions are severe and measurement noise is relatively low.

The single grid implementation of the exponential reconstructor was successful in that it produced results comparable to and sometimes slightly better than the least squares reconstructor. In addition, the exponential reconstructor on the single grid geometry developed here does not produce any significant component of the waffle mode. This is a distinct advantage over other wave front reconstruction methods that may prove to be very useful in practice.

SPGD algorithm approach for controlling the DM

The basic outline of the SPGD simulation performed is shown in Figure 1. A plane wave is propagated to the telescope aperture. The field at the aperture does not change for 6000 iterations of the algorithm while it converges on that particular realization of the atmosphere. The result is a PSF obtained from the last iteration of the algorithm. This process was repeated for 100 independent realizations of the atmosphere. Simulations were run at θ_z = 67 deg for the Maui3 turbulence profile and also for twice the Maui3 profile. This was done in order to test the algorithm in the most severe conditions for which performance was better in comparison to the phase reconstructors studied. The choice for the performance metric J is a weighted encircled energy of the PSF given by

$$J = \sum_x \sum_y P_r(u,v) PSF(u,v) e^{-\sqrt{x^2+y^2}/3}$$

where P_r is a pupil with a 3 pixel radius. This performance metric favors the intensity of the PSF to be at the center with an exponential roll off which is similar to the diffraction limited PSF. Use of this weighting function is an interesting variation on the previously published SPGD techniques, which have used a top hat function for P_r that improves speed, but reduces performance. The laboratory experiment is shown schematically in Figure 1.

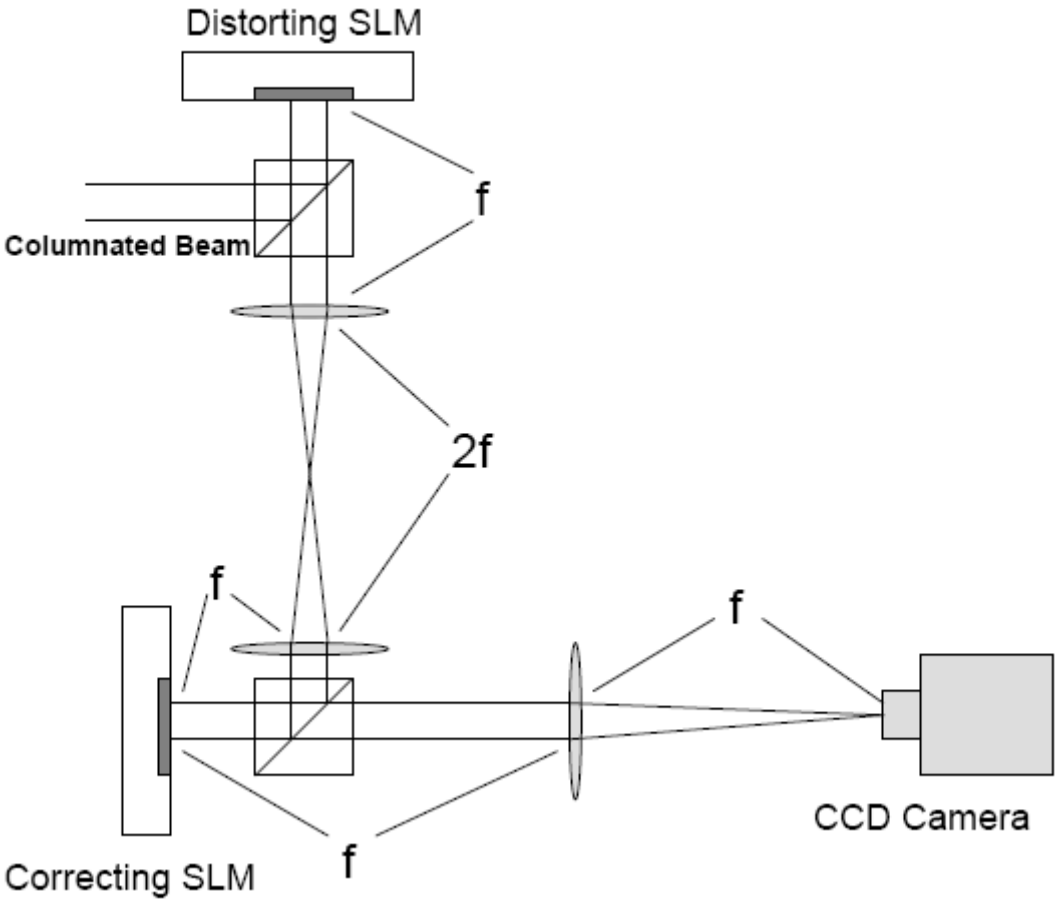

Figure 1. Schematic diagram of the SPGD experiment.

Key results from the SPGD study are presented in Figures 2, 3, and 4. The SPGD experiment was first used to study performance of the algorithm for fixed phase screens with varying *r*0. The physical size of *r*0 on the distorting SLM is arbitrary, so the sampling for the phase screens was chosen to be *dx* = 7.5 mm
making the 512 × 512 phase screen written to the SLM 3.84 m wide, even though the physical size of the SLM is much smaller. This makes the actuator separation of the 32 × 32 images written to the correcting SLM 12 cm. *r*0 values were chosen with respect to

the 3.84 m wide 512 $\times$ 512 phase screens written to the distorting SLM. The algorithm was tested with $r0$ varying from 4 cm to 50 cm with respect to the 12 cm SLM actuator separation. Each trial was run for 100 independent phase screens. In order to compare performance, the ratio of integrated intensity inside the first zero of the diffraction limited spot to the total integrated intensity was computed. This was chosen because it is a measure relative to the total intensity.

This experiment planning and execution was affected by the limited dynamic range of the camera. The camera must pick up low intensity levels outside the central spot, but the center of the spot can not be allowed to saturate. For each value of $r0$, neutral density filters were used to control the brightness of the central spot. The mean encircled energy and standard deviations from the sample of 100 phase screens are shown in Figs. 2 and 3 The standard deviations for the encircled energy are as large as 10%, but with 100 PSFs to average, the 95% confidence interval of the mean is $\pm$ 2%. While the data is not accurate enough to depict small changes, the overall trend is clear that performance increases as $r0$ increases from 4 cm to 10 cm and then plateaus at about $r0$ = 10 cm. This is reasonable since the actuator separation is 12 cm with respect to the phase screen sampling. Once the actuator separation becomes smaller than $r0$, the sampling is adequate enough to achieve a maximum performance.

The experimental set up for testing the SPGD algorithm was also used to test convergence with moving phase screens. A 1024 $\times$ 1024 phase screen was generated with $r0$ = 20 cm corresponding to the actuator separation of 12 cm. The phase screen written to the distorting SLM is a 512 $\times$ 512 cut from the larger 1024 $\times$ 1024 phase screen. The distorting SLM is timed to update once per iteration of the algorithm such that the section of the large phase screen written to it progressively moves from left to right. This was done for a range of speeds from 4 iterations per pixel shift to 50 iterations per pixel shift. Linear interpolation was used to update the SLM with a new partially shifted phase screen every iteration of the algorithm. Once the algorithm converged, a PSF was saved every 100 iterations from 1500 iterations to 2000 iterations so that 6 PSFs were obtained from each moving phase screen. This process was then repeated for 30 independently generated phase screens. The final result is a sampling of 180 PSF images obtained as described.

Figure 4 shows the radially averaged PSFs obtained from each speed of moving phase screens along with uncompensated and diffraction limited PSFs. Note that the uncompensated PSF is much worse than all the compensated PSFs, and the compensated PSFs approach the width of the diffraction limited PSF. From these plots it can be seen that the tails of the PSF become close to zero and the encircled energy rises above 50 percent at around 20 to 30 iterations per pixel shift of the phase screen. As an example, with the phase screen sampling taken to be 7.5 mm in the telescope pupil, and a wind speed of 10 m/s, the algorithm would need to run at about 27 KHz to attain 20 iterations per pixel shift.
The results presented in this chapter demonstrate the feasibility of various phase correction techniques in severe turbulence.

The key result of the wave front reconstruction simulations is that the implementation of the exponential reconstructor developed here has proven to be a good candidate for use in severe turbulence conditions and low light levels. The performance is better than that of the widely used least squares reconstructor and previously proposed implementation of the exponential reconstructor with Hartmann wave front sensor data. Also, the

difference in performance of the single grid implementation of the exponential reconstructor as compared to the other reconstructors studied gets larger as the zenith angle increases and as the measurement noise increases. In addition to the exponential reconstructor, the SPGD algorithm was also shown to be a viable choice for phase correction in severe conditions. If the turbulence strength causes *r*0 to be less than the wave front sensor subaperture size, SPGD can perform better than wave front reconstruction techniques. The experimental data also shows the SPGD algorithm can converge with changing turbulence conditions.

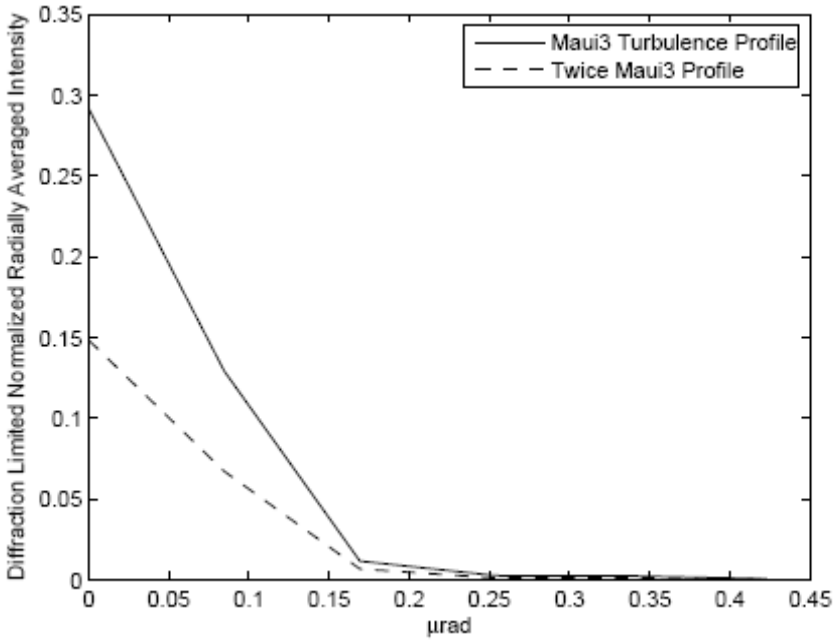

Figure 2. Average PSF over 100 iterations of the SPGD algorithm with θ_z = 67 for the Maui3 turbulence profile and also double the Maui3 profile.

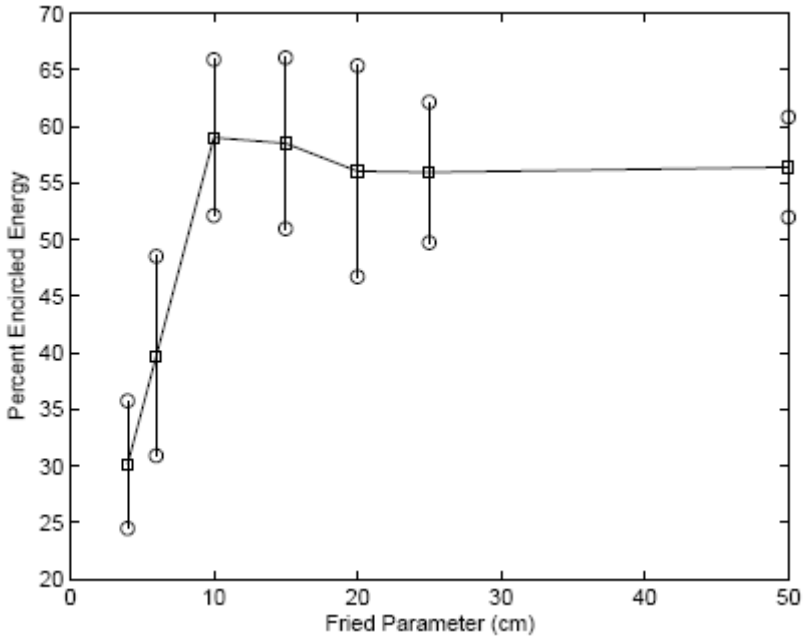

Figure 3. Percent of energy within the first zero of the diffraction limited PSF for fixed phase screens. 100-sample mean with standard deviations shown.

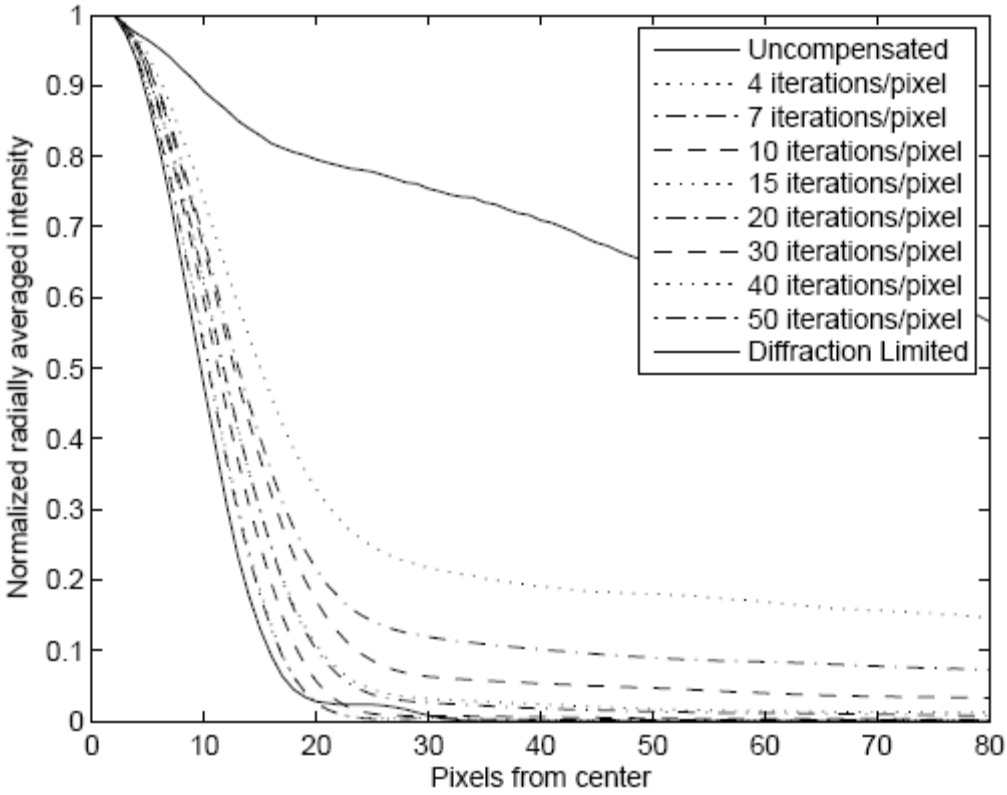

Figure 4. Radially averaged PSF for different speeds of moving phase screens.

Image reconstruction

As noted previously, as the zenith angle of the observations increases, the quality of the adaptive optics correction decreases, and as a result the quality of the imagery also decreases. Figure 5, which shows the average of four sequential images measured at a zenith angle of 70 degrees, illustrates this effect. We implemented an expectation-maximization (EM) algorithm-based multi-frame blind deconvolution image reconstruction technique to apply to the simulated data. A dissertation on this subject is presently still underway, and will be provided upon completion. An example reconstruction based on processing just these four images is shown in Fig. 6. Inspection of Fig. 6 shows that the reconstruction has sharper edges than the raw data, but suffers artifacts arising from the fact that the frames were measured closely spaced in time, and only four frames were processed.

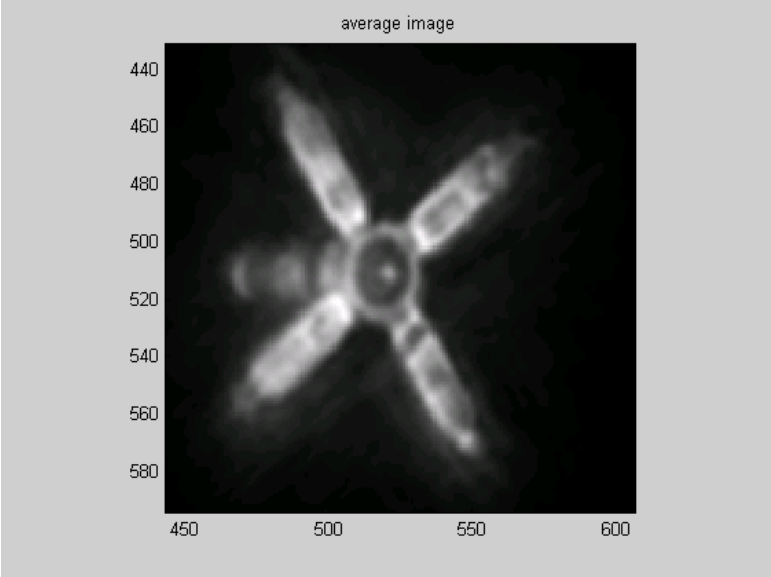

Figure 5. Average of four simulated images of the OCNR satellite measured through Maui3 turbulence at 70 degree zenith angle.

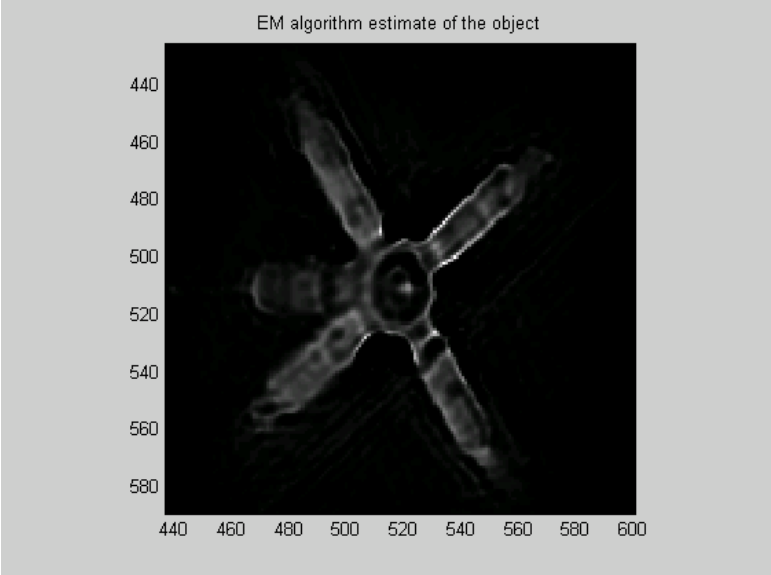

Figure 6. Results of 1000 EM iterations applied to the four frames used to calculate Fig. 5.

Conclusion

This effort has lead to the development and evaluation of new deformable mirror algorithms for adaptive optics system operation at high zenith angles, where suboptimal performance is expected with existing adaptive optics wave front reconstructors. The algorithms developed here are suitable for testing on the new adaptive optics system being developed for the AEOS telescope, though no plans for conducting such a test exist now.